RSC Advances

ROYAL SOCIETY OF CHEMISTRY

www.rsc.org/advances

Design of oxygen sensing nanomaterial: Synthesis, encapsulation of phenylacetylide substituted Pd(II) and Pt(II) *meso*-tetraphenylporphyrins into poly(1-trimethylsilyl-1-propyne) nanofibers and influence of silver nanoparticles

Emel Önal[a], Zeynep Ay[b], Zübeyde Yel[a], Kadriye Ertekin[b], Ayşe Gül Gürek[a], Sevinc Zehra Topal[*a] and Catherine Hirel[*a]

[a] *Gebze Technical University, Faculty of Science, Department of Chemistry, P. O. Box 141, Gebze, 41400 Kocaeli, Turkey*

[b] *Dokuz Eylul University, Faculty of Science, Department of Chemistry, 35160, Buca, Izmir, Turkey*

Abstract

Room temperature phosphorescent oxygen sensors have been designed by embedding symmetric palladium(II) or platinum(II) *meso*-tetraphenylporphyrins in poly(1-trimethylsilyl-1-propyne) in form of nanofibers along with silver nanoparticles. These materials combine the advantages of the high oxygen sensitivity of porphyrins and enhanced surface area of porous nanofibers. Phenylacetylide bearing Palladium (II) or platinum(II) *meso*-tetraphenylporphyrins (**Pd-TPA**, **Pt-TPA, Pd-TPP** and **Pt-TPP**) were designed to enhance phosphorescence quantum yields as well as sensitivity towards oxygen. Their syntheses were achieved by 2 alternative methods including successive metallation reaction and Sonogashira coupling via optimization of the synthetic strategies and conditions. The respective effect of the metal (Pd or Pt) and substituent on phosphorescence quantum yield as well as other photophysical properties was considered. The sensing performances of the corresponding silver–free and silver doped nanofibers were tested in the oxygen concentration range of 0.0 - 100.0 %. The offered composites provided the advantages of fast response, enhanced sensitivity, reversible and long lasting response, higher Stern-Volmer constants (K_{SV}) and low limit of detection values extending to 7.5 ppm for the oxygen.

Keywods: Oxygen sensor, Phosphorescence, Electrospun nanofiber, Silver nanoparticle, Palladium(II), Platinum(II), *meso*-Porphyrin, Phenylacetylide, Poly(1-trimethylsilyl-1-propyne).

*Corresponding authors: chirel@gtu.edu.tr; sztopal@gtu.edu.tr

Introduction

Development of nano-scale chemical sensors has been emerged as one of the most important research areas over the past decades[1, 2] as the physicochemical properties of bulk materials depend essentially of their size. Reducing materials from macro-to nano-scale increases the surface-to-volume ratio, influencing the photophysical and photochemical properties, which are important parameters on the development of chemical sensors. Nanomaterials show unique surface chemistry, thermal and electrochemical properties which can help to improve the sensor characteristics such as sensitivity, response time and limit of detection. Recently, fabrication of nanofibers and nanoscale beads has been studied to improve optical sensing properties[1-5]. Their porous structure with enhanced surface area, feasibility of modification and reliable entrapment of fluorescent dyes within the cavities made them useful especially for gas sensing studies[6-10].

On the other hand, accurate measurement of oxygen levels is of great importance in many process-control systems, strict inert gas atmospheres in semiconductor production, nuclear or life science studies, environmental and biomedical analysis as well as in industrial processes. The demanded oxygen concentration measurement range may vary from trace levels to large amounts depending on the application. Both, optical and electrochemical sensing approaches can measure the oxygen levels. Actually, scientists and instrument designers privileged optical sensing technology to overcome the electrochemically sensing devices problems such as slow response, frequent calibration required, suffering from electrical interference and large sample sizes required.

Luminescence-based oxygen sensors work on the principle of fluorescence or phosphorescence quenching of different types of organic dyes in oxygen permeable solid matrices[11]. Especially, palladium(II) and platinum(II)tetraphenylporphyrins have been widely used in phosphorescence-based oxygen sensors[12, 13] owing to their easy synthesis, strong and long-lived room temperature near infrared (NIR) phosphorescence and also high sensitivity even at low oxygen concentrations.[14] However, there are a few porphyrin-based optical O_2 sensor studies have been performed in nanoscale[12-17] where decrease of material size magnifies the sensitivity, photostability and working

range. Especially, *meso*-tetraphenylporphyrins are candidates of choice as their molecular structure can be efficiently and simply tuned by modifying the number, position, and nature of the functional groups introduced onto the (*meso*-)phenyl substituent. Therefore synthetic modification of such important dyes seems worthwhile to ameliorate the oxygen sensing properties. Among the available library of O_2 sensing molecules, such as palladium, platinum or iridium complexes, the one containing phenylacetylide substituent[18] has shown interesting phosphorescent and lifetime enhancement which led us to design symmetric palladium(II) and platinum(II) *meso*-tetraphenylporphyrins substituted by phenyl acetylide moieties as oxygen probe molecules (**Pd-TPA; Pt-TPA**).

Poly(1-trimethylsilyl-1-propyne) [poly(TMSP)] polymer matrix along with perfluorochemical additive (PFC) has previously attracted our attention for its high permeability *versus* oxygen $O_2(g)$[19]. All these developments prompted us to investigate the preparation of pioneering poly(TMSP)-based nanofibers including **Pd-TPA** or **Pt-TPA** by electrospinning method to obtain (**Pd-TPA)NF and (Pt-TPA)NF**. On the other hand, presence of the conducting metallic surfaces like gold and silver, affect emissive spectral properties of nearby fluorophores as demonstrated previously for $[Ru(bpy)_3]^{2+}$ dyes[20] and influence the sensitivity, photostability and calibration characteristics of oxygen sensors[21]. These studies encouraged us to investigate the effect of AgNPs on the nanofibers.

Herein, a detailed study about porphyrins including nanofiber preparation and their oxygen sensor properties in a large concentration range were reported. Poly(TMSP) matrix and targeted porphyrins (See Scheme 1) were suitable for electrospinning in presence of ionic liquid, silver nanoparticles (AgNPs) and perfluorochemical additive (PFC). As far as we know, this is the first study on phosphorescence-based oxygen sensing properties of porphyrins improved by silver nanoparticles. Moreover, the influence of phenylacetylide substituent on the Stern-Volmer quenching constant (Ksv), I_0/I_{100} and limit of detection (LOD) that are representative of the interactions between O_2 and the electrospun nanofibers were compared by studying the oxygen sensing properties obtained with palladium(II) and platinum(II)*meso*-tetraphenylporphyrin-based nanofibers ((**Pd-TPP)NF**; (**Pt-**

TPP)NF) as reference probes.

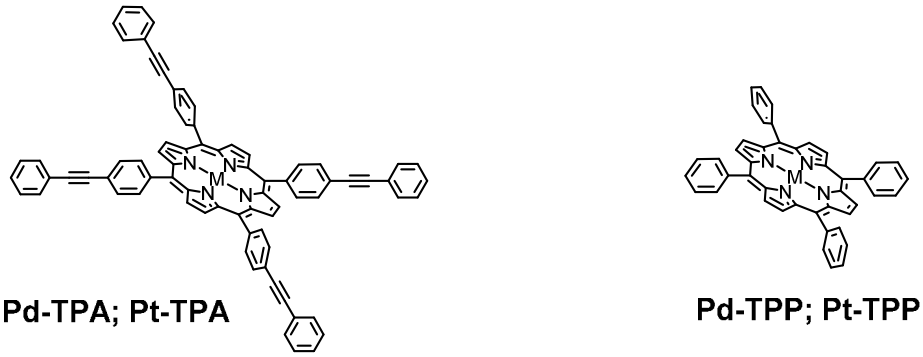

Scheme 1. Oxygen sensing probes (M=Pd, Pt) investigated in this study

Results and Discussion

This study was devoted to prepare nanoscale optical oxygen sensors. Our strategy was based on two main axes: i) incorporation of Pd(II) and Pt(II) *meso*-tetraphenylporphyrin complexes in poly(TMSP) matrix to obtain innovative oxygen sensing nanofibers combining room temperature phosphorescence and oxygen gas permeability, ii) tune of oxygen sensing properties of nanofibers by addition of silver nanoparticles.

Design and synthesis

In order to increase the oxygen sensing sensitivity and phosphorescence quantum yield of the dyes, novel *meso*-tetraphenylporphyrins (**TPP**) were designed by introducing phenylacetylide moieties at the *para*-position of the *meso*-phenyl substituent (**Pd-TPA; Pt-TPA**), a non-trivial feature, which provide a more rigid structure, enhance the π-conjugation and increase the luminescence properties at room temperature. The phosphorescence properties of Pd(II) and Pt(II) complexes at room temperature are of particular interest, but for such applications a large quantities of complexes have to be produced in an easy and efficient route. Two synthetic pathways (Scheme 2) were tested which both involve two sequential reactions, a metal insertion and a Sonogashira coupling in the reverse

order resulting to the formation of **Pd-TPA** and **Pt-TPA**. Both synthesis were started from the well-known *meso*-tetrakis(4-bromophenyl)porphyrin (**H_2-TPPBr)** as starting synthon, which can be easily prepared on a large scale following the Adler method[22]. *Method 1* involved first the metallation of **H_2-TPPBr** to obtain **Pd-TPPBr** and **Pt-TPPBr** followed by a Sonogashira coupling unlike *Method 2* was started by a Sonogashira coupling to obtain **H_2-TPA** and finished by metal insertion.

Among the range of Sonogashira coupling conditions, Cu-free cross coupling was preferred to avoid polymerization sub-products and metal insertion was improved by microwave irradiation heating.

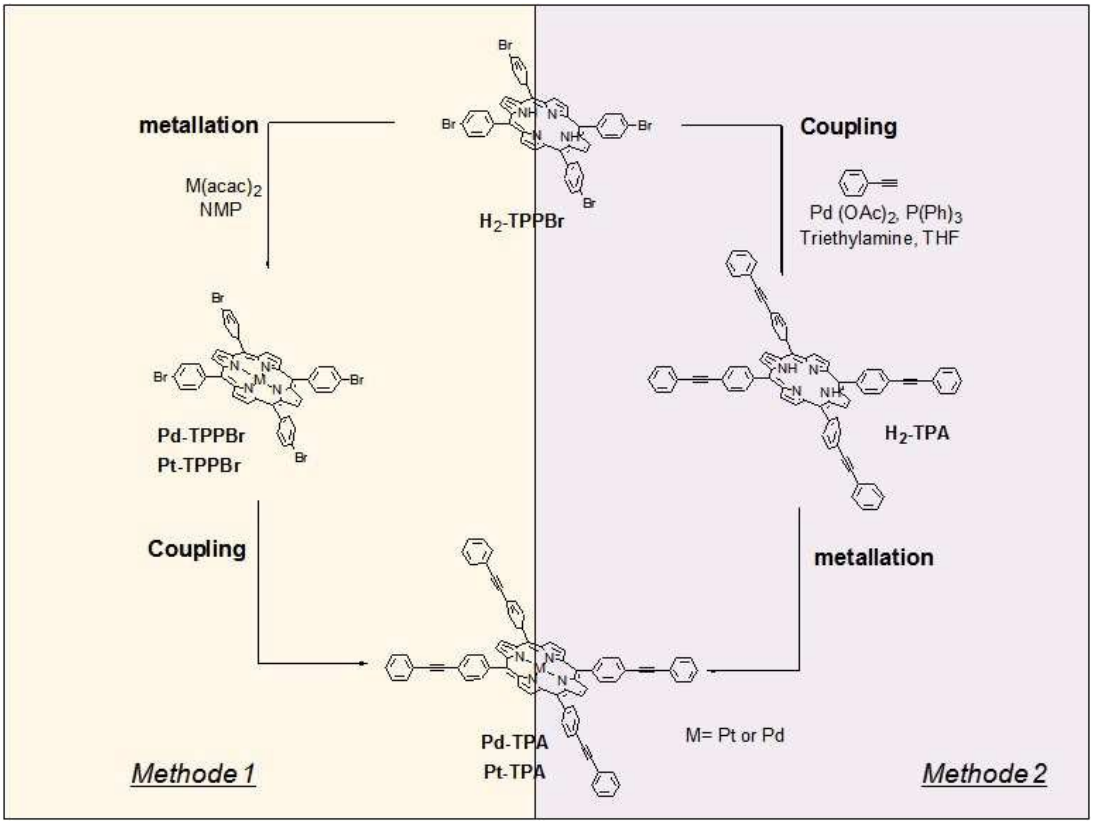

Scheme 2. Two-Steps synthetic strategies for **Pd-TPA** and **Pt-TPA**

Metal insertion. The limit to synthesize Pd(II) and Pt(II) metalloporphyrins lies in the slow rate incorporation of these transition metal ions into the porphyrin core, lowering drastically the reaction yield. To insert Pd(II), the classical approach is the use of Pd(II)chloride or acetate in refluxing DMF or benzonitrile with reaction times from 45 min. to days.[23, 24] Generally, Pt(II) insertion is more difficult and gives lower yield[25, 26] requiring refluxing for days in a degassed atmosphere. Reaction conditions were optimized against molar ratio of reagent, metal salt, organic solvent, heating (microwave assisted metallation or classical heating) to develop an efficient Pd(II) and Pt(II) insertion method.

Method 1 involved the metallation of **H_2-TPPBr** as substrate. Generally excess of metal salts is used; however this process spends a large amount of metal salts that are very expensive in bulk scale. When the molar ratio of metal salt:porphyrin is 2:1 or 2.5:1, yield decreases. The optimal ratio of metal salt:porphyrin is 3:1 (as observations in reports)[27, 28]. The choice of metal salt is crucial. Commercial availability, stability and ease of use of the metal salts were preferred. The metal salt should be enough soluble, but should not coordinate with the solvent of reaction thus competing with the porphyrin ring. $PtCl_2$ is a good example of unproper metal salt source that coordinates very fast in hot benzonitrile and can be easily isolated by precipitation with hexane[29, 30] Other disadvantage of halogen salts like $PdCl_2$ and $PtCl_2$, they are causing arcing in microwave field since they can be easily converted to metallic elements such as Pd^0 and Pt^0.[27] Among metal salt, $M(acac)_2$ salts are interesting because they are commercially available and highly soluble in weakly coordinating solvents. Our investigation compared $M(acac)_2$, MCl_2, M(OAc), and K_2PtCl_4 salt and the most efficient metal insertion was observed for $M(acac)_2$. Solvent should also be chosen very carefully as porphyrins and metal salts must be soluble in it. Moreover, for microwave heating, solvent must possess a high dielectric constant to drive the reaction more efficiently.[31] In this optic, *N*-methyl-2-pyrrolidinone (NMP) is an excellent choice due to its high polarity (6.7) and dielectric constant (32.2 at 25 ^oC). The results were summarized in Table S1 and S2. The best conditions were 3 equiv.

$Pd(acac)_2$/ NMP/ 180 °C/ MW 15 min. and 81% yield for **Pd-TPPBr** and 3 equiv. $Pt(acac)_2$/ NMP/ 110 °C/ MW 45 min. and 25% yield for **Pt-TPPBr.**

For *method 2*, the optimized metallation method was transposed to **H_2-TPA** substrate. Thanks to microwave power and adequate NMP solvent, **Pd-TPA** and **Pt-TPA** were obtained despite the weakness and reactivity of the triple bond (see Table 1). Especially, during the purification process, aggregation can easily occur and the use of usual technique such as precipitation in water or organic solvent has to be avoided.

Table 1: Pd(II) and Pt(II) metal insertion to **H_2-TPA**.

Equiv.	Metal salt	Organic solvent	Conditions	% yield
3	3 equiv. $Pd(acac)_2$	NMP	180 °C, MW, 30 min.	86
3	3 equiv. $Pt(acac)_2$	NMP	200 °C, MW, 45min.	52

Sonogashira coupling. Cu-free Sonogashira reaction conditions[32] were modified to obtained a controlled 4-fold coupling of phenylacethylene to **H_2-TPPBr** under the conditions outlined in **Scheme 2**. In *method 2*, The coupling reaction occurred with 84 % yield using $Pd(OAc)_2$, PPh_3, dry Et_3N and dry THF without purification problem. Unfortunately, when the same conditions adapted to *method 1*, it did not allow Sonogashira coupling of **Pd-TPPBr** and **Pt-TPPBr.** Regarding these results *method 2* was privileged.

Preparation and Characterization of Nanofibers

Although sensing compounds are of great importance in sensor design, the choice of the matrix is to be considered carefully in order to achieve desired sensor's characteristics. For example, matrix affects the gas diffusion rate which result in different relative signal change and response time. In

our preliminary work, according to the relative intensity change criteria (I_0/I_{100}), poly(TMSP) was found to be the ideal polymer matrix for porphyrin macrocycle in accordance with its moderate diffusion and partition coefficients.[19] On the other hand, the chemically and biochemically inert perfluorochemical (PFC); nonadecafluorodecanoic acid ($CF_3(CF_2)_8CO_2H$) was added to the preparation, called thereafter as cocktail, as oxygen solubility enhancing agent to increase the oxygen response of the sensing materials. Ionic liquids have been also utilized as additives to gain superior characteristics for the sensor materials such as high stability and sensitivity.[33] Presence of ionic liquid positively affects the nanofiber preparation process by increasing the electrical conductivity. In recent works, effect of the ionic liquid on porous nature of the nanofibers as well as oxygen sensing capabilities of the oxygen sensing molecule was studied. When 1-butyl-3-methylimidazolium tetrafluoroborate was added into the sensing composite, larger pores were handled compared to ionic liquid free ones.[34] Therefore, porous texture of nanofibers affects the response and recovery times as well as the sensitivity and selectivity of sensors. In this work, the fabrication of oxygen sensing nanofibers were achieved using poly(TMSP) matrix, optimum amount of PFC; 1.9×10^{-4} M (compared to cocktail weight) and 1-butyl-3-methylimidazolium tetrafluoroborate considering polymer/ionic liquid ratio in the literature.[34] On the other hand, to investigate the influence of AgNPs on phosphoresce-based oxygen sensitivity, AgNPs were also added to cocktails.

Various techniques can be used such as electrospinning, melt blowing, bicomponent spinning, force spinning and flash spinning. Electrospinning is a broadly used technique for electrostatic fiber formation which relies on repulsive electrostatic forces to produce nanofibers with diameter ranging from 2 nm to several micrometers.[35] Electrospinning has many advantages like ease of material combination, relatively low cost, ease of fiber deposition and handle of long and continuous fibers. To our knowledge, it is the first time that nanofibers of poly(TMSP) was prepared by electrospinning technique.

SEM and TEM imaging: The scanning electron microscope (SEM) images of **(Pd-TPA)NF** and **Ag-(Pd-TPA)NF** at various magnifications were shown in Fig. 1. The empty spaces of the holes within the network structures allow higher diffusion of O_2. It was observed that both electrospun membranes have a 3D network like structure with a random fiber orientation that was evenly distributed on the substrate. The diameters of the fibers varied between 283 and 727 nm for **(Pd-TPA)NF** and between 141 and 467 nm for **Ag-(Pd-TPA)NF**, respectively. The morphology of nanofibers was also investigated by Transmission electron microscopy (TEM). TEM images of **(Pd-TPA)NF** and **Ag-(Pd-TPA)NF** were shown in Fig. 1B and 1D. We can hypothesized from TEM pictures that the black spots localized on the surface of **Ag-(Pd-TPA)NF** correspond to AgNPs. This type of fibrous-structure provides higher surface area than thin films. Further increase of the surface area may be achieved by changing the conditions of the electrospinning process such as solvent composition, viscosity, concentration, temperature, humidity and working distance, which results in either smaller diameter fibers or increased porosity at the fiber surface.

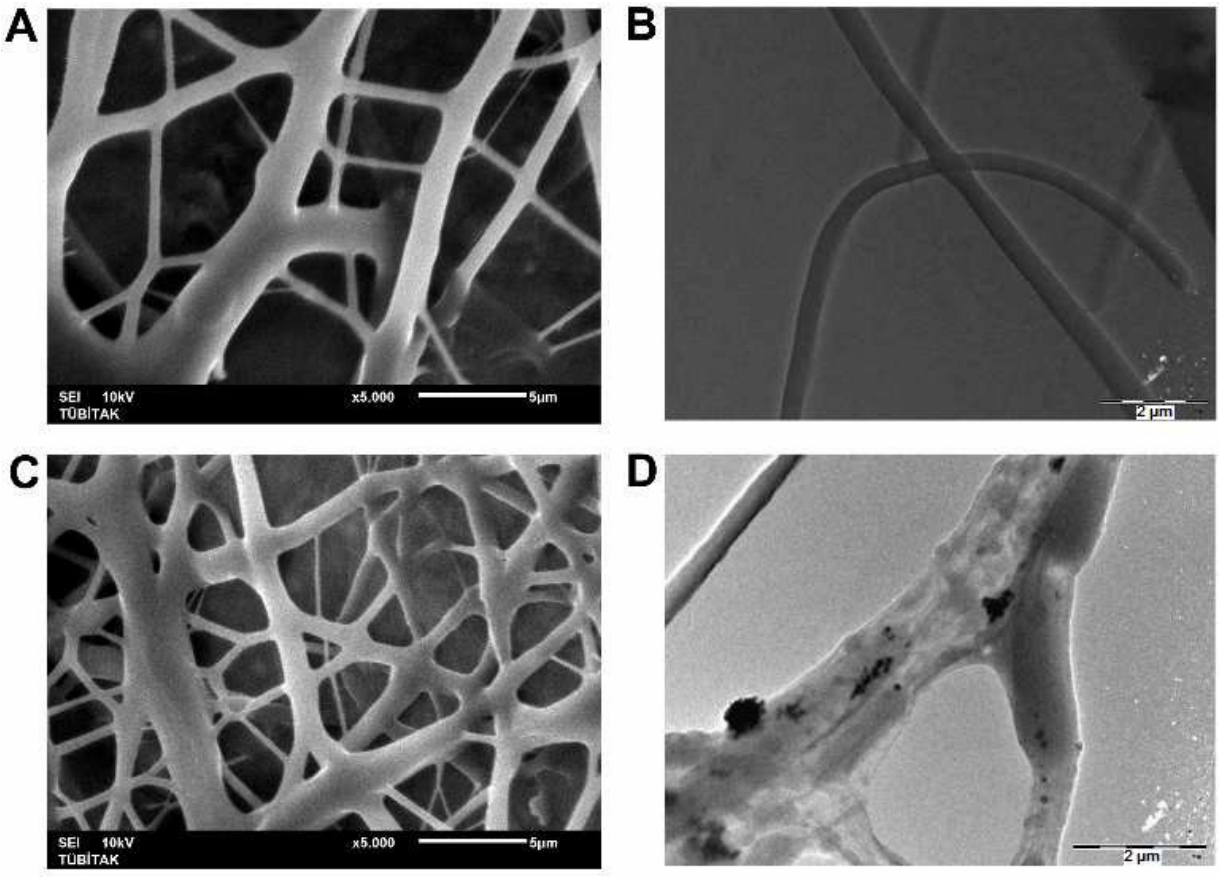

Figure 1. (A) SEM and (B) TEM images of **(Pd-TPA)NF**, (C) SEM and (D) TEM images of **Ag-(Pd-TPA)NF**.

Spectral Characterization

Absorption spectra of **Pd-TPP**, **Pt-TPP**, **Pd-TPA** and **Pt-TPA** were recorded in toluene solution and poly(TMSP) matrix. As expected, the absorption spectra exhibited a strong Soret band around 410 nm and two weak Q bands around 520 and 550 nm (see Fig. S27 and Table S3), with a 5-10 nm red shifts when porphyrin derivatives are incorporated in poly(TMSP) compared to toluene solution. The molar absorptivity coefficients of the Soret Bands which were in accordance with literature were 286 286± 596, 269 714± 5095, 104 881± 3024 and 130 962± 712 (n=3) for **Pd-TPP, Pt-TPP, Pd-TPA** and **Pt-TPA**, respectively (See Fig. S28, S29, S30 and S31).[36] All of the compounds obeyed

Beer's law in the concentration range of 2.0 x 10^{-6} - 8.0 x 10^{-6} M. It was observed that the phenylacetylide moieties decrease the ε values.

At room temperature, upon excitation around 420 nm, the molecules in deoxygenated toluene solutions exhibited strong NIR phosphorescence. **Pd-TPA, Pt-TPA, Pd-TPP** and **Pt-TPP** showed typical double phosphorescence bands with large Stoke's shifts (extending to 180 nm) that almost completely eliminates self-absorption of the emitted light (See Fig. S32, S33, S34 and S35). Luminescence-based data in solution phase and nanofibers were summarized in Table 2. The maximum phosphorescence excitation and emission wavelengths were similar for both the solution phase and the nanofibers.

Table 2. Phosphorescence spectra related data of the molecules in toluene and poly(TMSP) (λ_{ex} :excitation wavelength, $\lambda_{\max}^{em}$: maximum emission wavelength, $\lambda_{\max}^{ex}$: maximum excitation wavelength and Φ_P: phosphorescence quantum yield).

Compound	Medium	λ_{ex} (nm)	$\lambda_{\max}^{em1}$ (nm)	$\lambda_{\max}^{em2}$ (nm)	$\lambda_{\max}^{ex}$ (nm)	Φ_P
Pd-TPP	Toluene	415	698	771	421	0.054±0.002
	Poly(TMSP)	415	698	770	419	0.037±0.002
Pt-TPP	Toluene	415	664	731	398	0.185±0.01
	Poly(TMSP)	415	664	728	400	0.103±0.002
Pd-TPA	Toluene	420	704	770	428	0.025±0.01

	Poly(TMSP)	420	704	770	426	0.020±0.001
Pt-TPA	Toluene	420	670	734	406	0.092±0.005
	Poly(TMSP)	420	668	732	407	0.061±0.003

Phosphorescence quantum yields (ϕ_p) were calculated in toluene. **H_2-TPP** was used as a reference standard whose ϕ_F value is 0.12.[37] The Φ_P values of **Pd-TPP, Pt-TPP**, **Pd-TPA,** and **Pt-TPA** were found to be 0.054±0.002, 0.185±0.01, 0.025±0.01 and 0.092±0.005 in toluene, respectively. In parallel to molar absorptivity, phenylacetylide substitution resulted in nearly two fold decreased quantum yields. In contrast to the solution phase, in embedded forms, quantum yields did not exhibit any dramatic change. For both **TPP** and **TPA** derivatives, the platinum complexes exhibited higher quantum yield values.

Oxygen Sensing Properties

The phosphorescence emissions of metallo-porphyrin complexes decreased proportionally to the concentration of oxygen by dynamic quenching based on the energy transfer between the triplet state of the metal complex and the molecular (triplet) oxygen.[11] Quenching often is accompanied by the formation of singlet oxygen. However, herein we did not attempt to detect singlet oxygen. In the oxygen sensor, the relationship between intensity and the concentration of O_2 is reflected by the Stern-Volmer equation. The Stern-Volmer constant (K_{SV}) quantifies the quenching efficiency and therefore the sensitivity of the sensor. The O_2 sensitivity is also represented by the ratio (I_0/I_{100}), where higher value means higher sensitivity. For an ideal homogeneous environment like in

solution, the Stern-Volmer plots are linear. But, the Stern-Volmer plots for **(Pd-TPP)NF**, **(Pd-TPA)NF**, **(Pt-TPP)NF** and (**Pt-TPA)NF** exhibit downward curvature for the concentration range of 0.0-100.0 pO_2 typical of heterogeneous material. It means that porphyrin derivatives embedded into poly(TMSP)-based nanofibers are present in two different micro environments which possess different gas permeabilities, one being quenchable very efficiently, other either not being quenched at all or being quenched at a very different rate. The two-site model equation (Eq. (1)) is used to describe this kind of quenching behavior, and this equation can be used to calculate the two Stern-Volmer constants (K_{SV1} and K_{SV2}).[38]

The first and more intense phosphorescence emission maxima (λ_{max}^{em1}) were used to monitor the quenching of the excited state phosphorescence intensity by O_2.

$$\frac{I_0}{I} = \frac{1}{\frac{P}{1+K_{SV1}p_{O_2}} + \frac{1-P}{1+K_{SV2}p_{O_2}}} \qquad \text{Eq. 1}$$

In Equation 1, K_{SV1} and K_{SV2} were obtained for the same chromophores: where P accounts for fraction of nanofibers which can be interact with oxygen effectively, (1-P) presents for fraction of nanofibers which can't be interact with oxygen. In the equation, K_{SV2} was fixed as zero (K_{SV2}=0) to reduce the fit parameters, thus fitting excellently the nonlinear Stern-Volmer plots.[38] Calculated I_0/I_{100} parameters, K_{SV} and LOD values of all derivatives were summarized in Table 3. All of the Ksv parameters were given for the concentration range of 0.0 –100.0 % pO_2. Linear working ranges were also mentioned in Table 3. All of the nanofibers exhibited good Ksv values and high I_0/I_{100} parameters in the chosen matrix material. Varying the metal affected the oxygen sensitivity of the nanofibers. In all formulations, the Pd-based composites exhibited higher Stern-Volmer constants with respect to the Pt-based ones. However characteristics of the response were different in terms of the working range. The Pd derivatives exhibited dramatic drops and linear response when exposed to low concentrations of oxygen between 0.0-5.0% pO_2. The high Ksv values and I_0/I parameters were

the evidences of the extreme sensitivity of the Pd complexes to oxygen (See inset of Fig. 2A, Table 3). This kind of response make the Pd derivatives appropriate for the detection of trace amounts of oxygen. The Pt derivatives also exhibited good sensitivity to the oxygen in terms of K_{SV} and I_0/I values, but for larger concentration ranges (0.0–100.0% pO_2; See inset of Fig. 2B). Additionally the response was more linear than that of the response observed for the palladium derivatives.

When phenylacetylide substituents were introduced, small variations on the oxygen sensitivity were observed. As can be seen from comparing Fig. 3 and Fig. 2B, **(Pt-TPA)NF** yielded slightly higher K_{SV} (0.6374) with respect to **(Pt-TPP)NF** (0.4763). In case of the Pd derivatives, the Ksv value of the **(Pd-TPP)NF** was higher than that of the **(Pd-TPA)NF**.

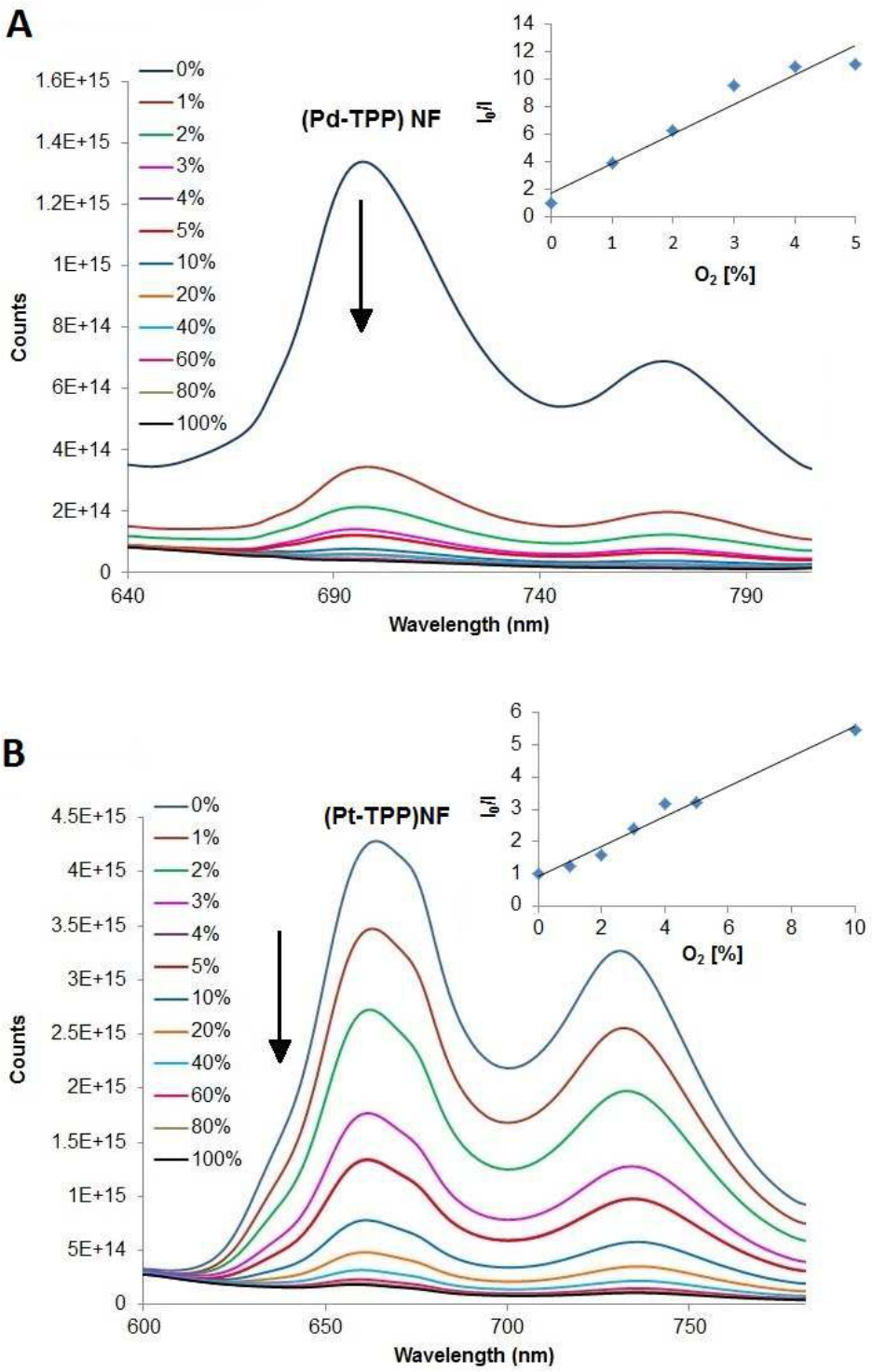

Figure 2. Oxygen induced emission spectra of **A) (Pd-TPP)NF, B) (Pt-TPP)NF** under small steps of O_2 (pO_2 %): 0.0, 1.0, 2.0, 3.0, 4.0, 5.0, 10.0, 20.0, 40.0, 60.0, 80.0, 100.0 %. Inset **A**: Linear working range of the sensing agent; [pO_2]%: 0.0-5.0 Inset **B**: [pO_2]%: 0.0-10.0.

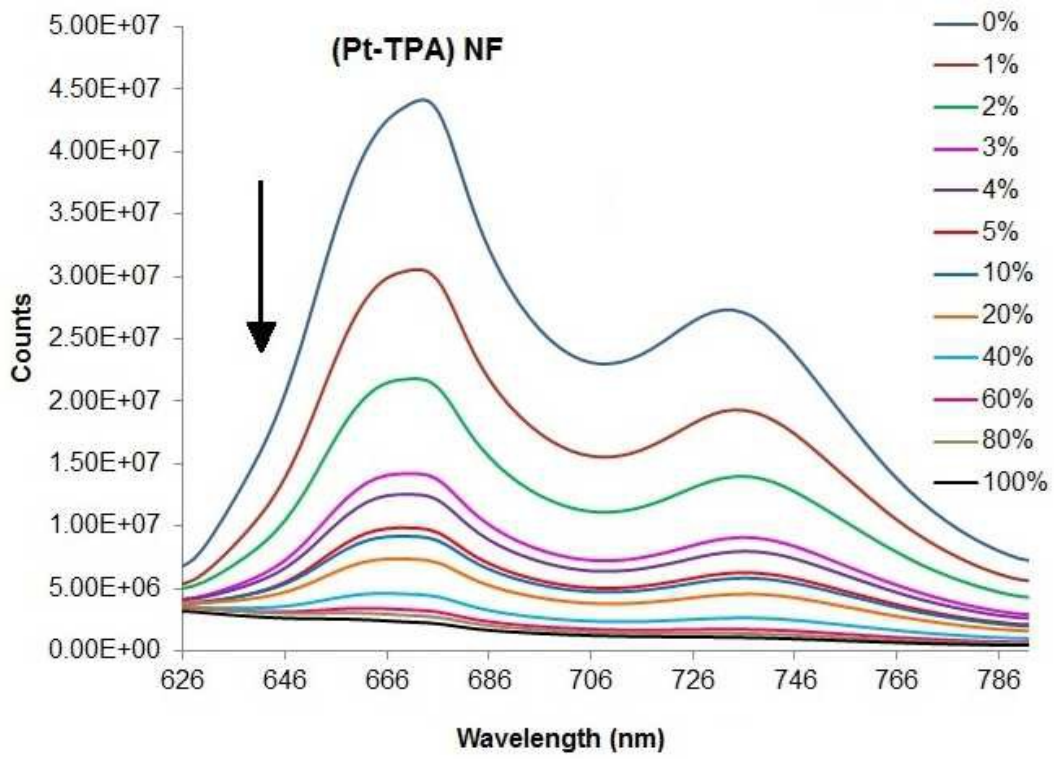

Figure 3. Oxygen induced emission spectra of **(Pt-TPA)NF** under small steps of O_2 partial pressures (pO_2 %): 0.0, 1.0, 2.0, 3.0, 4.0, 5.0, 10.0, 20.0, 40.0, 60.0, 80.0, 100.0 %.

Table 3. Phosphorescence emission wavelengths and oxygen sensitivities of the embedded molecules with/without AgNPs (I_0/I: parameter exhibit sensitivity; K_{SV}: Stern-Volmer coefficients, LOD: limit of detection).

Compounds in nanofiber form	λ_{max}^{em1} (nm)	λ_{max}^{em2} (nm)	I_0/I_{100}	K_{SV} ($\%^{-1}$)	LOD ($\%^{-1}$)
(Pd-TPP)NF	698	770	33.2	3.0584	0.00098
(Pd-TPA)NF	704	770	27.9	2.4854	0.0120
(Pt-TPP)NF	664	728	23.7	0.4763	0.0062

(Pt-TPA)NF	668	728	20.2	0.6374	0.0047
Ag-(Pd-TPP)NF	694	768	49.4	3.9823	0.00075
Ag-(Pd-TPA)NF	702	770	20.5	3.5073	0.0016
Ag-(Pt-TPP)NF	662	728	23.1	0.4339	0.0069
Ag-(Pt-TPA)NF	666	734	17.3	0.4165	0.0072

3.5. Effect of AgNPs additive

Effect of AgNPs on oxygen sensitivity was different for Pd and Pt derivatives. Fig. 4 reveals the response of **(Pd-TPA)NF** and **Ag-(Pd-TPA)NF**. Presence of the AgNPs enhanced the Ksv values of the **(Pd-TPP)NF** from 3.0584 to 3.9823 and of **(Pd-TPA)NF** from 2.4854 to 3.5073. Whereas the Ksv values of the platinum derivatives slightly dropped. Among them **Ag-(Pd-TPP)NF** exhibited the highest Stern-Volmer constant and I_0/I_{100} parameter (See Fig. S36-S38). The enhanced oxygen sensitivity of the silver doped composites can be attributed to the efficient interaction of surface plasmon polaritons of AgNPs with Pd complexes during oxygen induced collisional quenching. The competing surface plasmon absorption of the AgNPs with the excitation light (and following intrinsic emission of the silver) tunes the emission based response of the Pd derivatives. However, identification of the mechanism taking place in the solid state requires calculation of the Förster distances and/or transition dipoles and will be subject of further studies. The effect was not as significant for platinum porphyrin probes probably due to the lack of sensitivity induce by the metal effect (See Fig. 2).

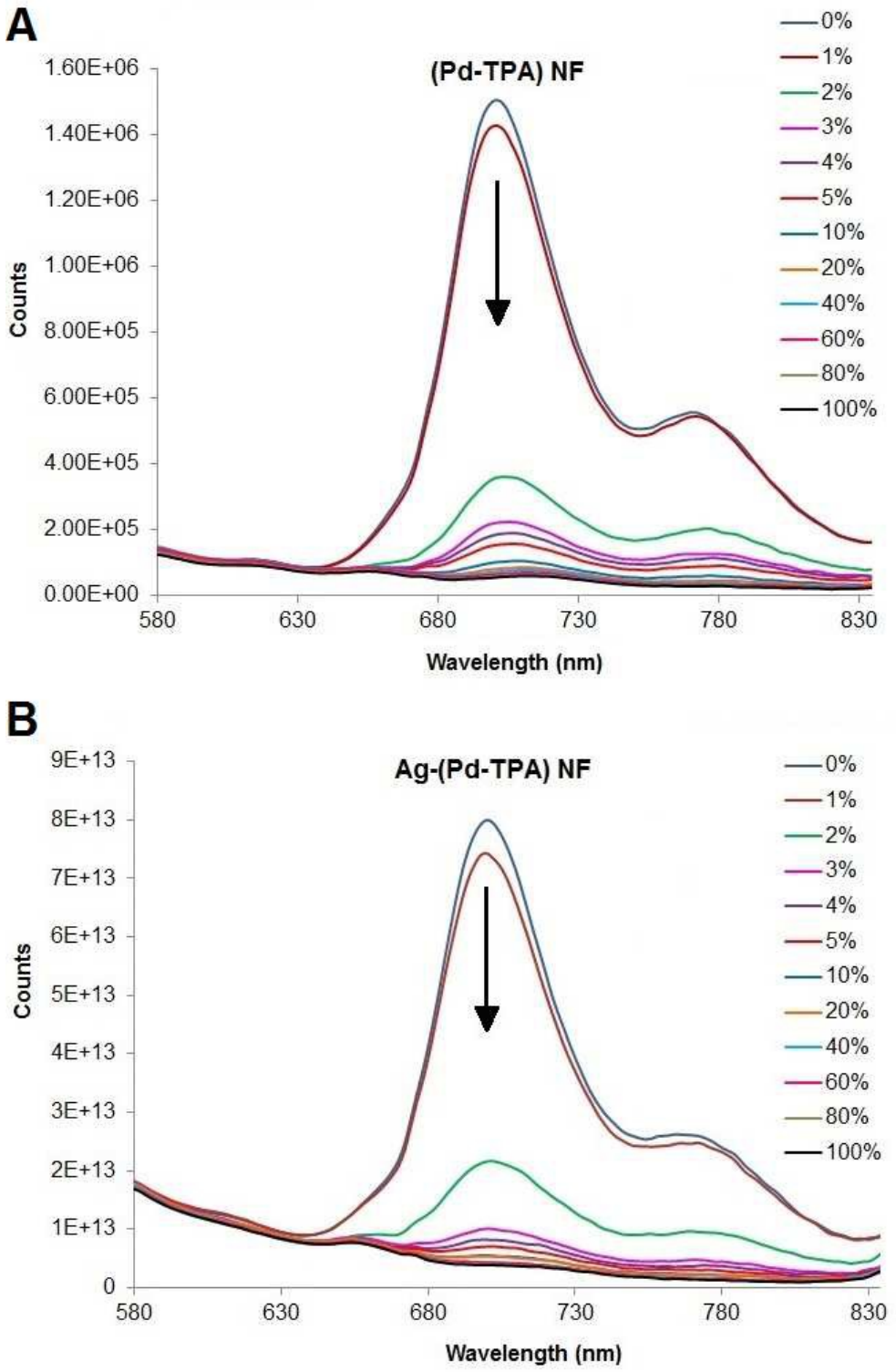

Figure 4. Oxygen induced emission spectra of **A) (Pd-TPA)NF, B) Ag-(Pd-TPA)NF** under O_2 partial pressures (pO_2 %): 0.0, 1.0, 2.0, 3.0, 4.0, 5.0, 10.0, 20.0, 40.0, 60.0, 80.0, 100.0%.

3.6. Limit of detection

LOD is governed by both the initial slope (K_{SV}) of the quenching plot and by the resolution of the instrument. Assuming a 0.1% uncertainty in light intensity measurement, the detection limit is $0.003/K_{SV}$ (K_{SV} expressed in $\%^{-1}$ units and at a signal-to-noise ratio of 3). The limit of detection (LODs) of the corresponding porphyrin-based nanofibers in the absence and presence of silver nanoparticles were determined by using the Stern–Volmer constants (See **Table 3**). Pd containing nanofibers exhibited better LOD values with respect to the Pt- based ones. In all cases presence of the silver nano particles enhanced the detection limit. Among the corresponding 8 nanofibers, the best LOD was found to be for **Ag-(Pd-TPP)NF** with the value of 0.00075% pO_2 (7.5 ppm).

3.7. Response time, regeneration time and repeatability

In all cases oxygen sensing responses of the porphyrin-based nanofibers were reversible. The variation of the phosphorescence emission changes of **(Pd-TPA)NF** and **Ag-(Pd-TPA)NF** under deoxygenated ($[O_2]$ =0.0%) and oxygenated conditions ($[O_2]$=100.0 % pO_2) were shown in Fig. 5. Similarly, reversible response characteristics of the **(Pt-TPA)NF** and **Ag-(Pt-TPA)NF** were shown in Fig. 6. **(Pd-TPA)NF** and **(Pt-TPA)NF** exhibited 13 and 18 % of signal drifts after 10^{th} cycle (See Fig. 5A and 6A). The drifts for (**Pd-TPP)NF** and (**Pt-TPP)NF** were 20 % and 18 %, respectively (See Fig. S39A and S40A). Addition of AgNPs negatively affected the regeneration cycles. The **Ag-(Pd-TPA)NF** and **Ag-(Pt-TPA)NF** lost 39 % and 32 % of their original signal intensity after second cycle (See Fig. 5B and 6B).

Response and regeneration times are defined as the time reach to 95 % of signal change when the gas is switched between O_2 partial pressures of 0.0 to 100.0 % pO_2. When the pO_2 sharply increased from 0.0 to 100.0%, the response times of **(Pd-TPA)NF** and **(Pt-TPA)NF** were found to be 6 and 5 seconds, respectively. The regeneration times of the same species were 117 and 46 seconds. On the other hand, (**Pd-TPP)NF** and (**Pt-TPP)NF** exhibited slightly longer response times of 13 and 6 seconds, respectively. Response and regeneration performances of **(Pd-TPP)NF**, **Ag-(Pd-TPP)NF,**

(Pt-TPP)NF, **Ag-(Pt-TPP)NF** were presented in Fig. S39 and S40. These values are likely to be limited by the time needed for the gas to flow-through tubing, in fact response and regeneration performances should be faster. In summary, response times of phenylacethylide substituted porphyrins were slightly faster than tetraphenylporphyrins. Besides, the addition of AgNPs into nanofibers did not affect the response and regeneration time. However, these response times were faster than that of PtTFPP incorporated into poly(2-hydroxyethylmethacrylate) (50 seconds),[39] but slower compared to that of PdTFPP and PtTFPP-based core shells (0.24 and 0.36 seconds, respectively).[15]

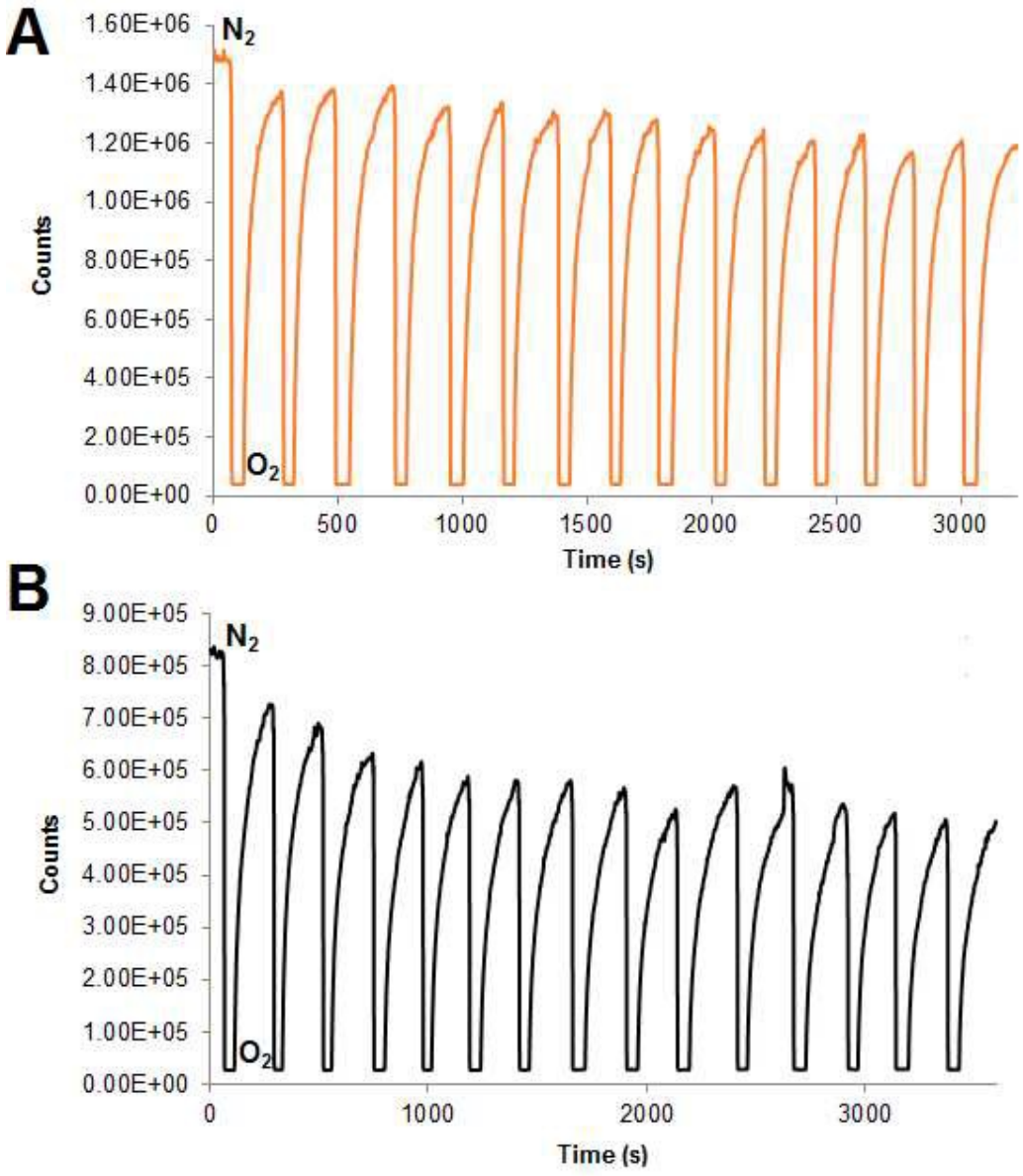

Figure 5. Time-based kinetic response of **A) (Pd-TPA)NF, B) Ag-(Pd-TPA)NF** in an alternating atmosphere of 100.0 % N_2 and 100.0 % O_2 .

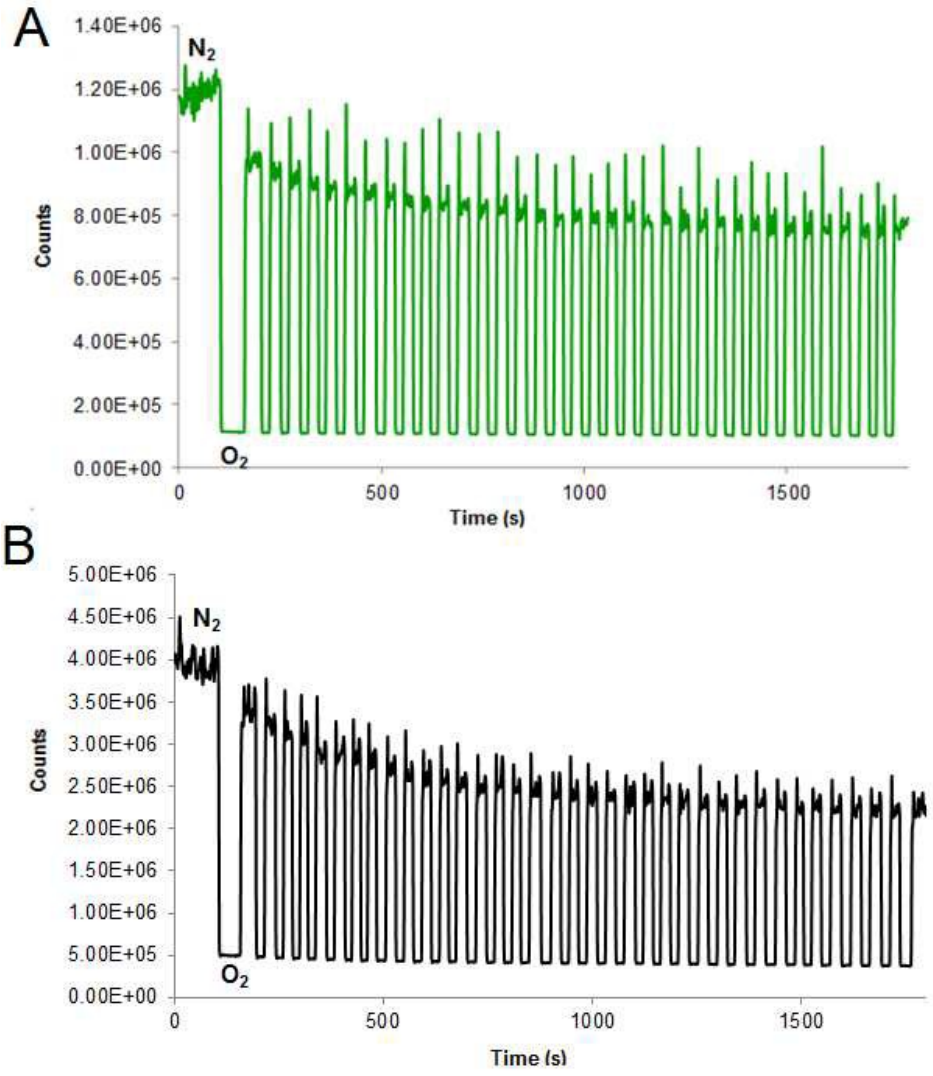

Figure 6. Time-based kinetic response of **A) (Pt-TPA)NF, B) Ag-(Pt-TPA)NF** in an alternating atmosphere of 100.0 % N_2 and 100.0 % O_2 .

3.8. Storage and stability

Concentration dependent oxygen responses of the sensing nanofibers were investigated for the 1st and 240th-days. The gathered concentration dependent oxygen response curves of **(Pd-TPA)NF, (Pt-TPA)NF, Ag-(Pd-TPA)NF** and **Ag-(Pt-TPA)NF** for 1st and 240th -days were presented in Fig. 7. Responses of **(Pd-TPP)NF, (Pt-TPP)NF, Ag-(Pd-TPP)NF** and **Ag-(Pt-TPP)NF** were presented in Fig. S41 and Fig. S42. After 240 days of period, **(Pd-TPP)NF** and **(Pt-TPP)NF** lost their original signal intensities by ~21% and 20%, whereas **(Pd-TPA)NF** and **(Pt-TPA)NF** were almost stable over 8 months stored under ambient conditions and in the absence of light. However, presence of AgNPs affected the reproducibility negatively. After 8 months, oxygen sensing signal changes (in terms of I_0/I_{100}) of the **Ag-(Pd-TPA)NF, Ag-(Pt-TPA)NF, Ag-(Pd-TPP)NF** and **Ag-(Pt-TPP)NF** were lost 4%, 28%, 59% and 56%, respectively.

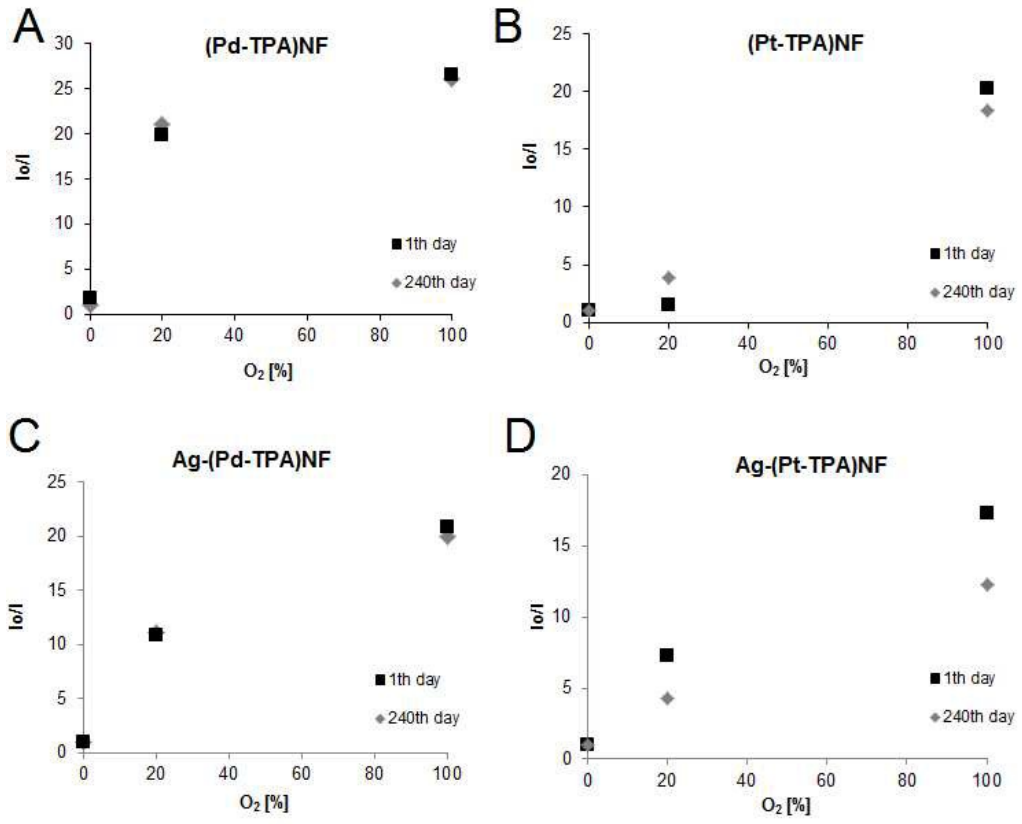

Figure 7: Storage stability test results of **A) (Pd-TPA)NF, B) (Pt-TPA)NF C) Ag-(Pd-TPA)NF** D) **Ag-(Pt-TPA)NF**.

4. Conclusion

In this study, **Pd-TPA** and **Pt-TPA** were designed to improve the phosphorescence oxygen sensing properties of porphyrin dyes. The synthesis, characterization and oxygen sensitivities of four different symmetric palladium(II) and platinum(II) *meso*-tetraphenylporphyrins were successfully achieved in absence and presence of silver nanoparticles. Palladium(II) and Platinum(II) metallation of *meso*-tetraphenylporphyrins were obtained in good and reproducible yield using the combination of microwave irradiation, acetate salt and NMP as solvent. Palladium(II) and platinum(II) *meso*-tetraphenylporphyrins were studied both in solution phase and in polymeric nanofibers obtained using electrospun technique. As far as we know, it is the first time that nanofibers of poly(TMSP) have been prepared by this technique.

The influences of metals (Pd or Pt) as well as variation of the substituent moieties were investigated. All nanofibers exhibited sensitive, reversible and long lasting steady-state response to oxygen. Among them, (**Pd-TPP)NF** exhibited the highest oxygen sensitivity and its oxygen sensing response was greatly improved by adding AgNPs. Therefore, we envision that more O_2 sensing (**Pd-TPP)NF** can be obtained by tuning the size of the nanofiber and AgNPs. Also varying the amount of AgNPs should influence the oxygen sensing properties. Our further studies will be on this direction.

Experimental

The following abbreviations were used in this article and in the figures: *N*-methyl-2-pyrrolidone (NMP), dichloromethane (DCM), tetrahydrofurane (THF), *meso*-tetraphenylporphyrin (**H_2-TPP**), *meso*-tetrakis(4-bromophenyl)porphyrin (**H_2-TPPBr**), palladium(II) *meso*-tetrakis(4-

bromophenyl)porphyrin (**Pd-TPPBr**), platinum(II) *meso*-tetrakis(4-bromophenyl)porphyrin (**Pt-TPPBr**), poly(trimethylsilylpropyne) **[poly(TMSP)],** silver nanoparticles (**AgNPs**), palladium(II) *meso*-tetraphenylporphyrin (**Pd-TPP**), platinum(II) *meso*-tetraphenylporphyrin (**Pt-TPP**), *meso*-tetrakis(4-phenylethynyl)phenylporphyrin (**H_2-TPA**), palladium(II) *meso*-tetrakis(4-phenylethynyl)phenylporphyrin (**Pd-TPA**), platinum(II) *meso*-tetrakis(4-phenylethynyl)phenylporphyrin (**Pt-TPA**), Pd-TPP-based nanofiber **[(Pd-TPP)NF]**, Pd-TPP-based nanofiber in presence of silver nanoparticles **[Ag-(Pd-TPP)NF]**, Pt-TPP-based nanofiber **[(Pt-TPP)NF]**, Pt-TPP-based nanofiber in presence of silver nanoparticles **[Ag-(Pt-TPP)NF]**, Pd-TPA-based nanofiber **[(Pd-TPA)NF]**, Pd-TPA-based nanofiber in presence of silver nanoparticles **[Ag-(Pd-TPA)NF]**, Pt-TPA-based nanofiber **[(Pt-TPA)NF]**, Pt-TPA-based nanofiber in presence of silver nanoparticles **[Ag-(Pt-TPA)NF],** Stern-Volmer constant (Ksv), Acetylacetonate (acac), Acetate (OAc).

General information

Starting materials were of reagent grade quality, purchased from Aldrich for Pyrrole (reagent grade %98), from Merck for propionic acid, from Across Organics for *N*-methyl-2-pyrrolidone (NMP). Tetrahydrofurane (THF) was dried over Na, preparative separations were performed by biobeads SM-2 Resin (300–1180 μm mesh size) and silica gel column chromatography Merck-60 (43–63 mesh). TLC was done on aluminum sheets precoated with silica gel 60F254 (Merck). The microwave device (Milestone Inc.) operates at fixe frequency (2450 MHz). The equipment can control the temperature (up to 250^{o}C) in a range of power values from 0 to 1000 watt. The perfluorochemical; nonadecafluorodecanoic acid; ($CF_3(CF_2)_8CO_2H$) was purchased from Alfa Aesar. Poly(1-trimethylsilyl-1-propyne) was supplied from ABCR company. $NaBH_4$ and $AgNO_3$ were purchased from Merck. 1-butyl-3-methylimidazolium tetrafluoroborate was supplied from Fluka.

Physical Measurements

UV-Vis, Steady-state luminescence, IR, NMR, MASS, SEM and TEM measurements. UV-Vis spectra were recorded by using a Shimadzu 2101 UV-Visible spectrophotometer. Steady-state luminescence emission spectra were recorded using a FLS920 from Edinburg Instruments, using 1 cm fluorescence cuvette (Hellma, 117100F-10-40). IR spectral data between 4000 and 600 cm^{-1} were recorded using a Perkin Elmer 100 FT-IR spectrometer with an attenuated total reflection (ATR) accessory featuring a zinc selenide (ZnSe) crystal. ^1H NMR spectra were recorded on a Varian 500 MHz spectrometer (with the deuterated solvents as the lock and tetramethylsilane as the internal reference). MALDI-MS spectra were obtained using 2,5-dihydroxybenzoic acid as the MALDI matrix, acquired in linear modes with an average of 50 shots on a Bruker Daltonics Microflex mass spectrometer equipped with a nitrogen UV-Laser operating at 337 nm and ESI-MS spectra were recorded by Bruker Daltonics MicrOTOF mass spectrometer equipped with an orthogonal electrospray ionization (ESI) source. SEM images were obtained with JEOL 6510-LV JSM scanning electron microscope. TEM observations were performed on a JEOL 2000FX electron microscope at an acceleration voltage of 160 kV. TEM samples were prepared on mesh copper grids.

Luminescence quantum yield determinations. Absorbance and luminescence spectra of the sample (for example **Pd-TPA**) and a reference standard were measured three times under identical conditions (absorbance at both the excitation wavelengths were 0.05). In our study, *meso*-tetraphenylporphyrin **(H_2-TPP)** (Φ_F= 0.12 in toluene[40]) was used as reference standard. All solutions were thoroughly deoxygenated by pump and freeze follows by nitrogen bubbling through for 10 min for three times. The ratio of the luminescence of the sample to reference standard was compared to find out quantum yield.

Oxygen sensing measurements. Oxygen and nitrogen gases were mixed in the concentration range 0-100% in a gas diluter (Sonimix 7000A gas blending system). The total pressure was maintained at 760 Torr. The output flow rate of the gas mixture was maintained at 550 mL min^{-1}. Gas mixtures were introduced into the sensing agent containing cuvette via a diffuser needle under ambient conditions.

Synthetic Procedures

Synthesis of *meso*-tetraphenylporphyrin (H_2-TPP) and *meso*-tetrakis(4-bromophenyl)porphyrin (H_2-TPPBr)

meso-tetraphenylporphyrin **(H_2-TPP)** and *meso*-tetrakis(4-bromophenyl)porphyrin **(H_2-TPPBr)** were synthesized following Adler Method as described in literature[22] with 30% yield for **H_2-TPP** and 25% for **H_2-TPPBr**. [**H_2-TPPBr**] FT-IR ν (cm^{-1}): 3320 (NH), 3022-3058 (CH_{Ar}), 1472 (C=N), 1348-1390 (=C-N), 1011 (C-$H_{pyrrole}$), 964(C-$H_{porp.\ ring}$) , 782(C-$H_{pyr.\ ring}$), 724 (NH bending). ^1H NMR ($CDCl_3$), δ (ppm)= -2.94 (s, 2H, NH), 7.82 (d, 8H, $CH_{Ar\text{-}phenyl}$), 7.98 (d, 8H, $CH_{Ar\text{-}phenyl}$), 8.76 (s, 8H, $CH_{pyrrole}$). UV-visible ($CHCl_3$), λ_{max}(nm) = 418; 512; 547; 588; 644. Mass (ESI-MS, m/z): $C_{44}H_{26}N_4Br_4$ [calcd]: 930.3200, [found]: 930.6624 $[M]^+$.

***meso*-tetrakis(4-phenylethynyl)phenylporphyrin (H_2-TPA):** In tri-necked reaction flask, 2,5 g of **H_2-TPPBr** (2,7 mmol), 11 mg(0,05 mmol) of palladium(II) acetate and 40 mg of triphenlphosphine were dissolved in the mixture of degazed and dry triethylamine/THF solution (35 mL/25 mL) under argon. 2,5 mL (21,6 mmol) of phenylacethylene was added and the solution was refluxed at 91 ^oC for one night. 10 mL of water was added after cooling of the solution at room temperature. The resulting purple precipitate was filtered on büchner, and washed with hot water. Purification was achieved by column chromatography on silica gel with a gradient of eluent from acetone/hexane (1:2; 1:1), acetone, toluene/hexane (1:1) to toluene. Yield 84 %. FT-IR ν (cm^{-1}): 3306 (NH), 3032

(CH_{Ar}), 2216(C≡C), 1473 (C=N), 1347-1398 (=C-N), 1020 (C-$H_{pyrrole}$), 968(C-$H_{porp.\ ring}$) , 795(C-$H_{pyr.\ ring}$), 753 ($NH_{bending}$). ^{1}H NMR: δ (ppm), $CDCl_3$ = -2.75 (s, 2H, NH), 7.45 (m, 12H, $CH_{Ar\text{-}phenyl}$), 7.70 (d, 8H, $CH_{Ar\text{-}phenyl}$), 7.96 (d, 8H, $CH_{Ar\text{-}phenyl}$), 8.23 (d, 8H, $CH_{Ar\text{-}phenyl}$) 8.91 (s, 8H, $CH_{pyrrole}$) UV-visible ($CHCl_3$), λ_{max}(nm) = 418; 512; 547; 588; 644. Mass (MALDI-MS, m/z) : $C_{76}H_{46}N_4$ [calcd]: 1014.37, [found]: 1015.403 $[M+H]^+$.

Insertion of Pd(II) and Pt(II)

General procedure: In a schlenk tube 1 eqv. of free base porphyrin was dissolved in NMP (0.05 mM) and 3 eqv. of $Pd(acac)_2$ or $Pt(acac)_2$ was added at once (or two times for TPA derivatives). The reactions were achieved under microwave irradiation (see **Table 1**, **S1** and **S2**). The reaction was cooled to room temperature and NMP was removed under reduced pressure. The orange residue was purified on silica gel with different equivalent of hexane/DCM eluent system for **Pd-TPP**, **Pt-TPP,** **Pd-TPPBr** and **Pt-TPPBr**; and purified on bio-beads for **Pd-TPA** and **Pt-TPA** eluted by DCM, ethanol and ethyl acetate.

Pd-TPP: Eluent hexane/DCM 4:1. Yield 100%. IR ν (cm^{-1}): 3052 (CH_{Ar}), 1440 (C=N), 1363-1351 (=C-N), 1071 (C-$H_{pyrrole}$), 963(C-$H_{por.\ ring}$), 788(C-$H_{pyr.\ ring}$). ^{1}H NMR ($CDCl_3$), δ (ppm)= 7.71 (m, 12H, $CH_{Ar\text{-}phenyl}$), 8.17 (d, 8H, $CH_{Ar\text{-}phenyl}$), 8.80 (s, 8H, $CH_{pyrrole}$). UV-visible (Toluene), λ_{max} (nm) = 417; 524; 555. Mass (MALDI-MS, m/z): $C_{44}H_{28}N_4Pd$, [calcd]: 718.130, [found]: 719.947 $[M+H]^+$.

Pd-TPPBr: Eluent hexane/DCM 9:1, 3:1, 2:1 successively. Yield 81%. IR ν (cm^{-1}): 2922 (CH_{Ar}), 1449 (C=N), 1350 (=C-N), 1070 (C-$H_{pyrrole}$), 1007(C-$H_{por.\ ring}$) , 792(C-$H_{pyr.\ ring}$). ^{1}H NMR ($CDCl_3$): δ (ppm), 7.82 (d, 8H, $CH_{Ar\text{-}phenyl}$), 7.96 (d, 8H, $CH_{Ar\text{-}phenyl}$), 8.74 (s, 8H, CH_{pyrrol}) UV-visible ($CHCl_3$), λ_{max}(nm)= 418; 523, 644. Mass (MALDI-MS, m/z) : $C_{44}H_{24}N_4Br_4Pd$, [calcd]:1034.74 , [found]:1034.571$[M]^+$

Pd-TPA: Eluent DCM, ethanol and ethyl acetate. Yield 86%. IR ν (cm^{-1}): 2924 (CH_{Ar}), 1442 (C=N), 1352 (=C-N), 1075 (C-$H_{pyrrole}$), 1012(C-$H_{por.\ ring}$) , 794(C-$H_{pyr.\ ring}$). ^1H NMR ($CDCl_3$): δ (ppm), 7.36 (m, 12H, $CH_{Ar\text{-}phenyl}$), 7.61 (d, 8H, $CH_{Ar\text{-}phenyl}$), 7.88 (d, 8H, $CH_{Ar\text{-}phenyl}$), 8.09 (d, 8H, $CH_{Ar\text{-}phenyl}$) 8.79 (s, 8H, CH_{pyrrol}) UV-visible(Toluene), λ_{max}(nm)= 426; 526, 559. Mass (MALDI-MS, m/z) : $C_{76}H_{44}N_4Pd$, [calcd]: 1118.26, [found]: 1119.548 $[M+H]^+$.

Pt-TPP: Eluent hexane/DCM 4:1. Yield 73%. IR ν (cm^{-1}): 3053 (CH_{Ar}), 1440 (C=N), 1358 (=C-N), 1074 (C-$H_{pyrrole}$), 1016(C-$H_{por.\ ring}$), 794(C-$H_{pyr.\ ring}$). ^1H NMR ($CDCl_3$), δ (ppm)= 7.66 (m, 12H, $CH_{Ar\text{-}phenyl}$), 8.07 (d, 8H, $CH_{Ar\text{-}phenyl}$), 8.67 (s, 8H, $CH_{pyrrole}$). UV-visible ($CHCl_3$), λ_{max}(nm)= 402; 510; 540. Mass (MALDI-MS, m/z): $C_{44}H_{28}N_4Pt$, [calcd]: 807.80, [found] : 808.497$[M+H]^+$.

Pt-TPPBr: Eluent hexane/DCM 9:1, 3:1, 2:1, 1:1. Yield 25%. IR ν (cm^{-1}): 2919 (CH_{Ar}), 1455 (C=N), 1356 (=C-N), 1069 (C-$H_{pyrrole}$), 1009(C-$H_{por.\ ring}$) , 792(C-$H_{pyr.\ ring}$). ^1H NMR ($CDCl_3$), δ (ppm): 7.82 (d, 8H, $CH_{Ar\text{-}phenyl}$), 7.93 (d, 8H, $CH_{Ar\text{-}phenyl}$), 8.67 (s, 8H, CH_{pyrrol}) UV-visible ($CHCl_3$), λ_{max}(nm)= 402; 514, 543. Mass (MALDI-MS, m/z) : $C_{44}H_{24}N_4Br_4Pt$, [calcd]:1118.84 , [found]: 1119.857 $[M+H]^+$.

Pt-TPA: Eluent DCM, ethanol and ethyl acetate. Yield 52%. IR ν (cm^{-1}): 2919 (CH_{Ar}), 1462 (C=N), 1364 (=C-N), 1056 (C-$H_{pyrrole}$), 968(C-$H_{por.\ ring}$) , 796(C-$H_{pyr.\ ring}$). ^1H NMR ($CDCl_3$), δ (ppm): 7.05 (m, 12H, $CH_{Ar\text{-}phenyl}$), 7.46 (d, 8H, $CH_{Ar\text{-}phenyl}$), 7.83 (d, 8H, $CH_{Ar\text{-}phenyl}$), 7.73 (d, 8H, $CH_{Ar\text{-}phenyl}$) 8.68 (s, 8H, CH_{pyrrol}). UV-visible (Toluene), λ_{max}(nm)= 409, 515, 574. Mass (MALDI-MS, m/z): $C_{76}H_{44}N_4Pt$, [calcd]: 1207.32, [found]: 1208.710. $[M+H]^+$.

Synthesis of silver nanoparticles

The chemical reduction of silver salts to obtain silver nanoparticles was occurred by following Solomon description[41]. 30 mL (0.002M) of a large excess of $NaBH_4$ was used not only to reduce the ionic silver but also to stabilize the silver nanoparticles (AgNPs) apart from each other. After cooling $NaBH_4$ solution with an ice-bath, 10 mL of 0.001M $AgNO_3$ solution was added dropwise (about 1 drop/ second). The reaction mixture was stirred vigorously during the reaction. After 3 min the color changed to yellow. The clear yellow colloidal silvers were centrifuged to obtained solid silver nanoparticles, which were dried at room temperature under reduced vacuum. AgNPs average size was found to be 84.6 nm according to the size distribution analysis which was presented in Fig. S26A. UV-Vis spectra of AgNPs in THF was also recorded, see Fig. S26B. Absorption maxima were found at 454 nm with a shoulder at 427 nm.

Preparation of electrospun nanofibers

In the present paper, polymer-based solutions were referred as cocktails. The resulting cocktails were containing 120 mg of poly(1-trimethylsilyl-1-propyne), 1.5 mg of porphyrin, 0.5 mg of nonadecafluorodecanoic acid, 25 mg of 1-butyl-3-methylimidazolium tetrafluoroborate and 2 ml THF. Electrospinning technique was used to fabricate nanofibers. The homogeneous polymer solutions were placed in a 10 mL plastic syringe fitted with a metallic needle of 0.4 mm of inner diameter. The syringe was fixed vertically on the syringe pump and the electrode of the high voltage power supply was clamped to the metal needle tip. The feed rate of polymer solution was 1.0 mL/h, the applied voltage was 25 kV and the tipto- collector distance was 10 cm. Nanofibers or porous structures were completely coated on the clean aluminum foil. For preparation of AgNPs supported cocktails, 2 mg of AgNPs were added to sensing cocktails.

Appendix A. Supplementary data

Supplementary data containing full spectroscopic characterization of all porphyrins(MALDI, ESI Mass, NMR and FT-IR spectroscopies), absorption, phosphorescence and oxygen sensing spectra associated with this article can be found free of charge on the RSC Publications website at DOI:

Author Contributions

The manuscript was written through contributions of all authors. All authors have given approval to the final version of the manuscript.

Notes

The authors declare no competing financial interest.

Acknowledgements

The authors thank TÜBİTAK for financial support (project number: **111M139**). Yann Bretonnière (ENS-Lyon; Quantum yield measurements) and Ozlem Oter (Dokuz Eylul University; Nanofiber preparation) are acknowledged for collaboration and fruitful discussions.

References

1. D. Aussawasathien, J. H. Dong and L. Dai, *Synthetic Metals*, 2005, **154**, 37-40.
2. J. Shi, Y. Zhu, X. Zhang, W. R. G. Baeyens and A. M. García-Campaña, *TrAC Trends in Analytical Chemistry* 2004, **23**, 351-360.
3. X.-d. Wang, R. J. Meier and O. S. Wolfbeis, *Adv. Funct. Mater.*, 2012, **22**, 4202-4207.
4. B. Ding, M. Wang, J. Yu and G. Sun, *Sensors* 2009, **9**, 1609-1624.
5. A. Lobnik and S. K. Urek, *Journal of Nano Research*, 2011, **13**, 99-110.
6. Y. Wang, B. Li, Y. Liu, L. Zhang, Q. Zuo, L. Shi and Z. Su, *Chemical Communications*, 2009, DOI: 10.1039/B910305H, 5868-5870.
7. X. Lu and M. A. Winnik, *Chem. Mater.*, 2001, **13**, 449-3463.
8. H. Xu, J. W. Aylott, R. Kopelman, T. J. Miller and M. A. Philbert, *Anal. Chem.*, 2001, **73**, 4124-4133.
9. S. M. Borisov, T. Mayr and I. Klimant, *Anal. Chem.*, 2008, 573-582.
10. M. Z. Ongun, O. Oter, G. Sabancı, K. Ertekin and E. Celik, *Sensors and Actuators B, Chemical*, 2013, **183**, 11-19.
11. X.-d. Wang and O. S. Wolfbeis, *Chemical Society Reviews*, 2014, **43**, 3666-3761.
12. S. M. Borisov, P. Lehner and I. Klimant, *Analytica Chimica Acta*, 2011, **690**, 108-115.
13. V. S. Tripathi, G. Lakshminarayana and M. Nogami, *Sensors and Actuators B: Chemical*, 2010, **147**, 741-747.
14. T.-w. Sunga and Y.-L. Lo, *Sensors and Actuators B, Chemical*, 2012, **173**, 406-413.

15. R. Xue, C. Ge, K. Richardson, A. Palmer, M. Viapiano and J. J. Lannutti, *ACS Applied Materials & Interfaces*, 2015, **7**, 8606-8614.
16. S. M. Borisov, C. Larndorfer and I. Klimant, *Adv. Funct. Mater.*, 2012, **22**, 4360-4368.
17. R. Xue, P. Behera, J. Xu, M. S. Viapiano and J. J. Lannutti, *Sensors and Actuators B, Chemical*, 2014, **192**, 697-707.
18. H. Guo, S. Ji, W. Wu, W. Wu, J. Shao and J. Zhao, *Analyst*, 2010, **135**, 2832-2840.
19. S. Z. Topal, E. Önal, K. Ertekin, O. Oter, A. G. Gürek and C. Hirel, *J. Porphyrins Phthalocyanines*, 2013, **17**, 431–439.
20. J. R. Lakowicz, Y. Shen, S. D'Auria, J. Malicka, J. Fang, Z. Gryczynski and I. Gryczynski, *Analytical Biochemistry*, 2002, **301**, 261-277.
21. O. Ozturk, O. Oter, S. Yildirim, E. Subasi, K. Ertekin, E. Celik and H. Temel, *Journal of Luminescence*, 2014, **155**, 191-197.
22. A. D. Adler, *J. Org. Chem.* , 1967, **32**, 476-477.
23. J. W. Buchler, in *The Porphyrins*, ed. D. Dolphin, Academic Press, New York, 1978, vol. 1, pp. 389-483.
24. in *The Porphyrin Handbook*, eds. K. M. Kadish, K. M. Smith and R. Guilard, Academic Press, New York, 2000, vol. 3, pp. 26-27.
25. L. M. Mink, M. L. Neitzel, L. M. Bellomy, R. E. Falvo, R. K. Boggess, B. T. Trainum and P. Yeaman, *Polyhedron*, 1997, **16**, 2809-2817.
26. L. E. Helm, L. I.; Merbach, E., , *Helv. Chim. Acta.* , 1984, **67**, 1453-1460.
27. M. L. Dean, J. R. Schmink, N. E. Leadbeater and C. Bruckner, *Dalton Trans.*, 2008, DOI: 10.1039/B716181F, 1341-1345.
28. N. Gunawardhana and M. Tabata, *Environ Chem Lett*, 2011, **9**, 473-477.
29. S. M. Borisov, G. Zenkl and I. Klimant, *ACS Applied Materials & Interfaces*, 2009, **2**, 366-374.
30. S. M. Borisov and I. Klimant, *Dyes and Pigments*, 2009, **83**, 312-316.
31. A. de la Hoz, A. Diaz-Ortiz and A. Moreno, *Chemical Society Reviews*, 2005, **34**, 164-178.
32. W. B. Austin, N. Bilow, W. J. Kelleghan and K. S. Y. Lau, *The Journal of Organic Chemistry*, 1981, **46**, 2280-2286.
33. S. Z. Topal, K. Ertekin, D. Topkaya, S. Alp and B. Yenigul, *Microchim Acta*, 2008, **161**, 209-216.
34. O. Oter and G. S. Sahin, *Turkish Journal of Chemistry*, 2015, **39**, 395-411.
35. N. Bhardwaj and S. C. Kundu, *Biotechnology Advances*, 2010, **28**, 325-347.
36. C. Rimington, *Biochem. J.*, 1960, **75**, 620-623.
37. J. M. Dixon, M. Taniguchi and J. S. Lindsey, *Photochemistry and Photobiology*, 2005, **81**, 212-213.
38. F. Niedermair, S. M. Borisov, G. Zenkl, O. T. Hofmann, H. Weber, R. Saf and I. Klimant, *Inorg. Chem.* , 2010, **49**, 9333–9342.
39. F. Su, R. Alam, Q. Mei, Y. Tian, C. Youngbull, R. H. Johnson and D. R. Meldrum, *PLoS ONE*, 2012, **7**, e33390.
40. J. M. Dixon, M. Taniguchi and J. S. Lindsey, *Photochem. Photobiol.*, 2005, **81**, 212-213.
41. S. D. Solomon, M. Bahadory, A. V. Jeyarajasingam, S. A. Rutkowsky and C. Boritz, *Journal of Chemical Education*, 2007, **84**, 322-325.